Opposite trends in the microstructural evolution of irradiated ceramics driven by asymmetric defect migration energies

A. Debelle, J.-P. Crocombette, A. Boulle, E. Martinez, B. Uberuaga, D. Bachiller-Perea, L. Thome, M. Behar

HAL Id: cea-02410178

https://cea.hal.science/cea-02410178

Preprint submitted on 11 Jun 2020

Opposite trends in the microstructural evolution of irradiated ceramics driven by asymmetric defect migration energies

A. Debelle*[1,2], J.P. Crocombette[2], A. Boulle[3], E. Martinez[4], B.P. Uberuaga[4], D. Bachiller-Perea[1],

L. Thomé[1], M. Béhar[5]

1. CSNSM, Université Paris-Sud, CNRS/IN2P3, Université Paris-Saclay, 91405 Orsay, France.
2. CEA, DEN, SRMP, Université Paris-Saclay, 91191 Gif-sur-Yvette, France.
3. SPCTS, CNRS UMR 7315, Centre Européen de la Céramique, 12 rue Atlantis, 87068 Limoges, France.
4. Materials Science and Technology Division, Los Alamos National Laboratory, Los Alamos, New Mexico 87545, USA.
5. Instituto de Física, Universidade Federal do Rio Grande do Sul, C.P. 15051, 91501-970 Porto Alegre, RS, Brazil.

Abstract

X-ray diffraction experiments complemented with numerical simulations reveal that two ceramic oxide materials, c-ZrO_2 and MgO, under similar ion irradiation conditions, exhibit an unexpected, opposite response with varying the irradiation temperature. In fact, the final damage state is reached faster in c-ZrO_2 with increasing temperature than in MgO. Rate equation cluster dynamics simulations show that defect clustering is favored in c-ZrO_2 while defect annealing is enhanced in MgO. This contrasting behavior can be rationalized in terms of the asymmetry in the interstitial *vs*. vacancy defect migration energies. We demonstrate that these trends allow qualitatively reproducing the evolution with temperature of the experimental disorder.

*Corresponding author: aurelien.debelle@u-psud.fr

Keywords: irradiation; migration energy; X-ray diffraction; rate theory; disorder

The modification of matter upon interaction with energetic particles usually arises through the energy loss of the incident particles to the atomic nuclei and/or to the electrons of the target [1]. This process, referred to as irradiation, may lead to defect generation and subsequent microstructural changes. These effects may have beneficial or detrimental implications in many fields of applied materials science such as advanced electro-optical devices [2-4], engineered nanostructures [5-7], strain engineering [8-10], nuclear materials [11-13] and space exploration [14,15]. The physical phenomena underlying the damage build-up under irradiation have been the focus of research for several decades, but there is still a need for comprehensive studies at moderate or high temperatures that correspond to most of the in-service conditions of actual relevance.

In the context of ceramics, important for many of the applications above, much work has focused on the behavior of materials that undergo amorphization upon irradiation, typically at lower temperatures. The effect of the irradiation temperature on the threshold fluence for such a phase change to occur has been, for instance, particularly scrutinized, mainly in oxides and carbides. The primary observation was a delay or even a complete suppression of the amorphization process with increasing temperature owing to enhanced dynamic defect annealing (see e.g. these comprehensive papers [16-18]). In contrast, studies of ceramics that retain their crystalline structure under irradiation are much scarcer [19-22]. Among these materials, cubic (yttria-stabilized) zirconia (c-ZrO_2) and magnesia (MgO), which have been examined in a wide temperature range, exhibit an unexpected, opposite response in irradiation-induced damage build-up [23,24] with increasing temperature.

Cubic zirconia and magnesia are two materials that have received particular attention, owing to their potential applications in nuclear energy (both fission and fusion) [25,26], and, in the case of zirconia, as solid oxide fuel cells for high-energy-density portable power supplies [27]. The two materials exhibit significant differences such as the crystalline structure and the ionicity of the bonding (MgO having higher ionic character). However, at a fixed temperature, they behave similarly under ion irradiation: in both materials, one observes a continuous damage accumulation process

which starts with point defect creation and culminates with the formation of a network of tangled dislocation lines [23,28]. The two materials do not undergo a phase change and they both retain their crystalline character. This process is the same irrespective of the temperature. Nonetheless, strikingly, the two materials exhibit an opposite behavior with respect to their response to changing the irradiation temperature [23,24]. Indeed, as partially demonstrated by Rutherford backscattering spectroscopy in channeling mode (RBS/C), with increasing temperature, the accumulation of disorder is accelerated in c-ZrO$_2$ but it is slowed down in MgO. In fact, RBS/C permitted the determination of the fluence at which there is a dramatic change in the defect nature, namely from small point defect clusters to dislocation loops [23,24]. This change is frequently referred to as a second step in the damage accumulation process and the corresponding transition fluence decreases with temperature for c-ZrO$_2$ while it increases for MgO. This result is illustrated in Fig.1 of the Supplemental Material [29].

In the present Letter, we rationalize this unexpected and opposite behavior in the two materials with respect to the irradiation temperature and correlate it with the dissimilar diffusivities of the irradiation-created defects. We performed X-ray diffraction (XRD) measurements that indicate an even more subtle difference because the behavior in temperature is shown to depend on the fluence (i.e. number of ions per unit surface). The experimental results are qualitatively reproduced using Rate Equation Cluster Dynamics (RECD) calculations which allow us to conclude that the key property that leads to the different damage accumulation kinetics is the asymmetry of the defect migration energies between vacancies and interstitials.

{100}-oriented c-ZrO$_2$ and MgO single crystals were irradiated with MeV Au ions, respectively (the nuclear and electronic energy losses where equivalent for both materials). Irradiations at 80 K were performed at the Instituto de Fisica of the Universidade Federal of Rio Grande do Sul, while irradiations at elevated temperatures were carried out at the SCALP facility [30]. More details can be found in [23] for c-ZrO$_2$ and in [24] for MgO. Ion fluences ranged from 5x10^{12} to 5x10^{15} cm^{-2} for c-ZrO$_2$

and from 5×10^{12} to 2×10^{14} cm^{-2} for MgO. The same ion flux, 5×10^{11} cm^{-2}.s^{-1}, was used for irradiations of both materials.

The XRD measurements were performed with a Philips X'Pert PRO MRD diffractometer equipped with a standard Cu tube. A monochromatic (Cu K$_{\alpha 1}$ radiation) and parallel beam was obtained by using a multilayer mirror at the output of the tube followed by a four-reflection Ge(220) monochromator in asymmetric configuration; the resulting primary-beam divergence is ~18 arcsec (0.005°). A three-reflection Ge(220) crystal analyzer was placed in front of the detector to improve the angular resolution. Symmetric θ-2θ scans were recorded in the vicinity of the (400) Bragg reflection of the rock salt magnesia structure (2θ~94.058°) and of the fluorite zirconia structure (2θ~73.575°). These θ-2θ scans were fitted with the dedicated RaDMaX program that allows one to obtain the strain and disorder depth profiles in irradiated materials [31]. The disorder, which is the parameter of interest in this work, is linked to the so-called static Debye-Waller (DW) factor that damps the coherent scattered intensity due to the presence of defects in crystalline regions [32 and references therein]. This disorder is directly related to the nature and density of the irradiation-induced defects. Note that when DW=1, the crystal is perfect and when DW→0, the crystal is severely defective. In the following, we plotted <(1-DW)$_{max}$> as a measure of the disorder level which has the advantage of increasing as the damage increases, improving the interpretability of the data. The average is performed over a +/- 50 nm wide region around the damage peak (MeV Au ions do not have a constant energy-loss over the entire projectile path) in order to smooth out fluctuations which are frequently observed in the XRD determination of this parameter [32].

Rate Equation Cluster Dynamics simulations treat, in an homogenous framework, the evolution of the concentration of a population of defect clusters formed by either vacancies or interstitials through rate equations. These equations describe the creation of single defects by irradiation, and the growth or shrinkage of clusters through the emission or absorption of mobile species, which are restricted to single defects in the present case. We used the 1D version of the CRESCENDO code; a complete description of this code can be found in [33,34].

A brief summary of the method is presented here, the reader is refereed to [33] and [34] for a complete description of the Crescedo code and to a previous study on zirconium carbide [SP] for a more detailed presentation of the present simulation set-up. Focusing for instance on interstitial clusters, the evolution of the concentration $C(I_n)$ of clusters I_n containing n interstitials is driven by the difference in growth flux from cluster I_{n-1} to I_n ($J_{I_{n-1} \to I_n}$) and shrinkage flux from I_{n+1} to I_n ($J_{I_{n+1} \to I_n}$). Each flux is the sum of two parts corresponding to the interstitial and vacancy mobile species. Both parts have a absorption component (governed by a factor β) and a thermal emission component (governed by a factor α), e. g. for the growth flux due to mobile interstitials :

$$J_{I_{n-1} \to I_n}^I = \beta_{n-1,I} C(I_{n-1}) C(I) - \alpha_{n,I} C(I_n) \tag{1.}$$

The absorption component depends on the concentrations of the captured mobile and capturing immobile species, whereas the emission efficiency depends only on the concentration of the immobile emitting species. The absorption factor

$$\beta_{n-1,I} = 4\pi Z_I D_I d_{I-I_{n-1}} \tag{2.}$$

In this expression D_I is the diffusion coefficient of mono-interstitials which depends on their migration energy, $d_{I-I_{n-1}}$ is the capture distance of an interstitial by a cluster of size n-1. The efficiency factor (Z_I=1.1) accounts for the elastic interaction between dislocations loops or lines and mono- interstitial. The elastic interactions of vacancies with clusters being comparatively negligible, this term does not appear in the corresponding equations for vacancies (Z_v=1) []. Detailed balance enforces a relation between β and α which involves the binding energy between the mono-interstitial and the cluster[].

The equation of evolution of the mobile mono-interstitials or vacancies is more complex, e.g. for interstitials I_1:

$$\frac{dC(I)}{dt} = G_I - \sum_{n>1} J_{I_n \to I_{n+1}}^I + \sum_{n>1} J_{V_n \to V_{n+1}}^I$$

$$+2 \left(\alpha_{2,I} C(I_2) - \beta_{1,I} C(I) C(I) \right) - 4\pi (D_I + D_V) d_{I-V} C(I) C(V) - \rho Z_I D_I C(I) \tag{3.}$$

The first term in the RHS of the equation is the source term which reproduces the production of defects by irradiation (see below). The penultimate term is the recombination flux which depends on the sum of the diffusion coefficients of interstitials and vacancies. The last term denotes the elimination of mobile interstitials on sinks of the microstructure. Finally, the other terms form the clustering fluxes of interstitials towards interstitials or vacancies clusters. The formation of a di-interstitial has a special form, the factor 2 coming from the fact that the two species which cluster are mobile

In order to apply the RECD framework to c-ZrO_2 and MgO, we had to make, rooted in the properties of zirconia and magnesium oxide, some simplifying assumptions that are discussed hereafter. First, we considered only the cationic sublattices because cations are the rate limiting species in the diffusion processes in c-ZrO_2 and, in this material, there is a significant concentration of structural oxygen vacancies in pristine crystals as a consequence of the yttrium stabilization. In MgO, the properties of both anion and cation defects are very similar [cite e.g. Uberuaga PRL], so there is no loss in generality just considering the cations. Second, we approximated the source term by a simple creation of monovacancies (V) and monointerstitials (I), and the rate of defect creation was determined from SRIM [35] calculations using 40 eV and 55 eV as threshold displacement energies for c-ZrO_2 and MgO, respectively. It is known that this code overestimates the rate of surviving defects (because for instance it does not consider intra-cascade recombination) [36,37]. A recent quantitative study of irradiation defects in MgO as a function of temperature indicates that the actual defect creation efficiency is in the range of a few percent; we hence divided the SRIM-predicted value by a factor of 10. Defect creation fluxes ($G_i=G_v$)were then 4×10^{18} cm^{-2}.s^{-1} for c-ZrO_2 and 1.9×10^{18} cm^{-2}.s^{-1} for MgO. We emphasize that, beyond the defect creation fluxes, the only difference between the models for c-ZrO_2 and MgO are the defect migration energies.
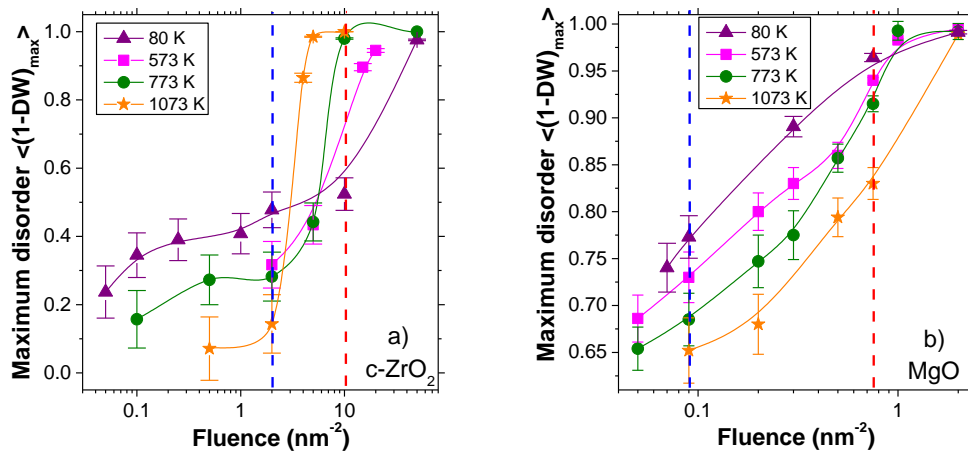
Figure 1: Disorder level, averaged over a window centered on the peak of the implanted damage profile, determined by fitting the XRD θ-2θ scans reported in [23] for c-ZrO$_2$ and provided in Fig. 2 of the Supplementary Material [29] for MgO. The disorder is given as a function of the ion fluence and at the indicated temperatures for a) c-ZrO$_2$ and b) MgO. In each figure, the blue line indicates results representative of a low fluence regime while the red line represents a high fluence regime.

Figure 1a shows the disorder level at the maximum of the damage profile for irradiated c-ZrO$_2$ single crystals as a function of fluence at four temperatures: 80, 573, 773 and 1073 K. An increase in the disorder is observed with increasing fluence irrespective of the temperature. However, for all temperatures, two regimes can be identified. At low fluence (less than ~2-3/nm^2) the disorder decreases with increasing temperature, while it increases with increasing temperature at fluences greater than ~2-3/nm^2. This point is highlighted when examining the values of disorder at two particular fluences indicated by the vertical dashed lines in Fig. 1a (the blue line is at 2 nm^{-2} and the red line is at 10 nm^{-2}). It is thus worth mentioning that the higher the temperature, the faster the final damage state, when the disorder saturates, is reached in this material. Note that in the present case complete disorder does not imply an amorphous structure: the samples retain their crystalline structure but the high level of disorder (due to extended defects in the crystalline matrix) extinguishes the coherent part of the diffraction signal which is redistributed as diffuse scattering around the Bragg peaks. Such diffuse scattering clouds are readily observed in reciprocal space maps of irradiated c-ZrO$_2$ and MgO [23,24].

Figure 1b shows the disorder level measured for irradiated MgO single crystals versus fluence and for the same four temperatures as for c-ZrO$_2$. The minimum disorder in MgO is higher than in c-ZrO$_2$ because of a lower intrinsic quality of the MgO crystals. Note that the investigated fluence range is smaller in MgO than it is in c-ZrO$_2$, but it is sufficient to catch the whole disordering process up to saturatrion. The trend in the disorder evolution with fluence is similar irrespective of the temperature with a progressive increase until complete disorder. One can observe a slight change in the slope of the disorder curves at intermediate fluences but overall, at a given fluence the disorder level decreases with increasing irradiation temperature over the entire fluence range. Therefore, similarly to zirconia, the disorder at low fluence decreases in magnesia with increasing temperature. However, opposite to c-ZrO$_2$, the level of disorder induced in MgO at higher fluence diminishes with increasing temperature. That is, the behavior of MgO is constant versus temperature: higher temperatures lead to less disorder, regardless of fluence. While this happens in c-ZrO$_2$ at low fluences, at high fluences, c-ZrO$_2$ exhibits the opposite behavior. Therefore, within the experimental uncertainty for some data points, the final damage state reached at high fluence always occurs sooner for lower temperature irradiations in MgO, in complete contrast to the result found in c-ZrO$_2$ (and despite a similar defect generation sequence occurring in both materials at fixed temperature [23,24,28]).

The hypothesis that was put forward to tentatively explain this major difference between these two materials was a difference in the effect of the irradiation temperature on the defect mobility [23,24]. In fact, if increasing temperature would obviously lead to an increase in the defect mobility in both materials, the clustering process was hypothesized to be favored in c-ZrO$_2$ whereas the recombination process would be enhanced in MgO. Guided by this assumption, we performed preliminary kinetic Monte Carlo simulations which strongly suggested that the asymmetry in the defect migration rate could indeed be the key factor to explain this opposite behaviour. In order to validate this hypothesis, we developed a methodology for RECD simulations to determine the effect of the defect energetics on the evolution of the defect distributions in the two materials.

Based on the data reported in the literature, we used the following values for the defect migration energies: 3 eV for both V and I in c-ZrO$_2$ [38,39], and 2 and 0.4 eV for V and I, respectively, in MgO [40,41]. Note that the value of 3 eV for c-ZrO$_2$ is a lower limit of values reported in the literature (all obtained with empirical potentials); values of 5-6 eV are mainly reported but with these high values, RECD simulations did not show any defect migration below 1200 K. There are thus two key differences in the defect diffusivity between the two materials: (i) defect mobility is larger in MgO than in c-ZrO$_2$ for both defects and, more importantly, (ii) the relative mobility of V and I is different in MgO but is similar in c-ZrO$_2$.

In a first step, we determined, by RECD, two reaction rates for both materials at different fluences for a wide range of temperatures: the recombination (rec) rate between I and V, and the interstitial clustering (clust) rate. Figure 2a shows, in addition to the defect source term, these two rates for c-ZrO$_2$ at two fluences, 1.5 and 10 nm^{-2} (these fluences are characteristic of the two regimes determined experimentally and defined by the vertical dashed lines in Fig. 1a). Although the rates start to be significant only at relatively high temperature (which is directly related to the large defect migration energies of 3 eV), it can be observed that for both fluences and for all temperatures, the clustering rate is larger than the rate for defect recombination. This result proves the assumption of favored defect clustering in c-ZrO$_2$. For MgO, reaction rates are given in Fig. 2b for fluences of ~0.05 and ~0.5 nm^{-2} (also characteristic of the two regimes identified for this material). Defect migration starts at a lower temperature than for c-ZrO$_2$ (due to the lower defect migration energies). Note the logarithmic Y-scale which indicates a large range in the defect clustering and recombination rates versus temperature. More importantly, the rate of defect recombination is much larger than that for defect clustering for both fluences. This result demonstrates that defect recombination is favored over defect clustering in MgO.

As highlighted in equation (4.) the terms appearing in the evolution of mono-defects can be divided in three parts : the clustering, elimination and recombination fluxes. The first two terms

(clustering and elimination) depend only on the coefficient diffusion of the considered mono-defect while the recombination depends on the sum of both diffusion coefficients. Furthermore the clustering term involves for interstitials a bias term (Z_I, see Eq2.) which effectively reproduces the attractive elastic interaction between interstitials and clusters. This bias term has proven to be fundamental in the modelling of the evolution of irradiation defects [43,44]. The present value of 1.1 is a reasonable assumption commonly used. The exact calculation of these bias needs involved elastic calculations[] and is far beyond the scope of our present qualitative treatment. Considering these equations, it can be observed that, for c-ZrO$_2$, the difference in the clustering and recombination rates is only due to this bias, which explains why the Y-scale is limited. More importantly, in MgO, interstitials are mobile well before vacancies are and therefore, the probability for a mono-interstitial to meet a mono-vacancy is high because the concentration of the latter is large as they diffuse much less and thus neither cluster nor eliminate. The recombination flux is therefore very high. As the recombination process takes place, the concentration of interstitials C_I drastically decreases and so does the clustering rate, explaining why it varies over several decades in MgO.
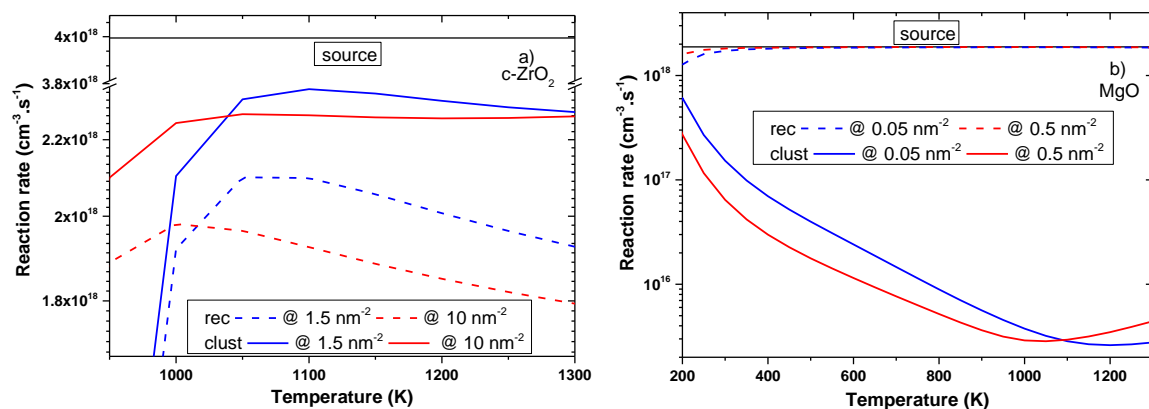

Figure 2: Source term for defects (horizontal black solid lines) and recombination (rec, dashed lines) and clustering (clust, solid lines) reaction rates as a function of temperature for both a) c-ZrO$_2$ and b)

MgO, at both low and high fluences characteristic of the two identified regimes in the damage accumulation process (see Figs. 1a and 1b).

The RECD simulations definitely show that the asymmetry in I and V mobility plays a crucial role in the defect accumulation process in irradiated c-ZrO$_2$ and MgO over a large range of temperatures, with a complete opposite trend in the two materials: enhanced defect clustering in the former and preferential defect recombination in the latter. But can this opposite trend be used to reproduce the evolution in the disorder as a function of the temperature and fluence for the two materials? To answer this question, we identified parameters obtained with RECD calculations that could be compared to the disorder level derived from XRD measurements. First, it is important to mention that the irradiated crystals are characterized by a tensile strain principally generated by the presence of interstitial defects, as demonstrated in [23,45]. Second, at low fluence, where small defect clusters that do not interact are dominant, the DW factor is proportional to the number of point defects in the clusters [46], while at high fluence, where dislocation loops form, the DW varies with the number of point defects in the loops to the power 3/2 [46]. Therefore, one reasonable way to compare XRD and RECD is to plot, for RECD, the total number of interstitials at low fluence, and at high fluence the number of interstitials inside clusters with a size larger than a threshold value (i.e. in dislocation loops). Based on transmission electron microscopy experiments, small dislocation loops of a few nm in diameter can be observed in these materials [23,28]. We decided to monitor, with RECD data, the number of interstitials in clusters containing at least 10 point defects; this value corresponds to clusters of ~1 nm in diameter, which is slightly smaller than experimentally observable, but represents a compromise between a reasonable experimental size and a size for which significant effects are observed in the RECD calculations. It is worth mentioning that this approach of using two different types of defects and thus two different criteria to evaluate disorder in the RECD simulations is also consistent with the RBS/C experiments that reveal that the transition from the first to the second step of the accumulation damage process is the transition from point defect clusters to dislocation loops of a significant size [23,24].

The XRD-derived disorder and the RECD-derived disorder in c-ZrO$_2$, as a function of temperature, are shown in Figs. 3a and 3b, respectively. In both cases, two fluences characteristic of the steps in the damage accumulation process have been selected (see the dashed lines in Fig. 1a). At low fluence, the XRD-derived disorder decreases with increasing temperature while at higher fluence, it increases. A qualitative agreement is found when looking at the disorder obtained from RECD calculations. In particular, two distinct and opposite dependencies with temperature for both characteristic fluences are reproduced.
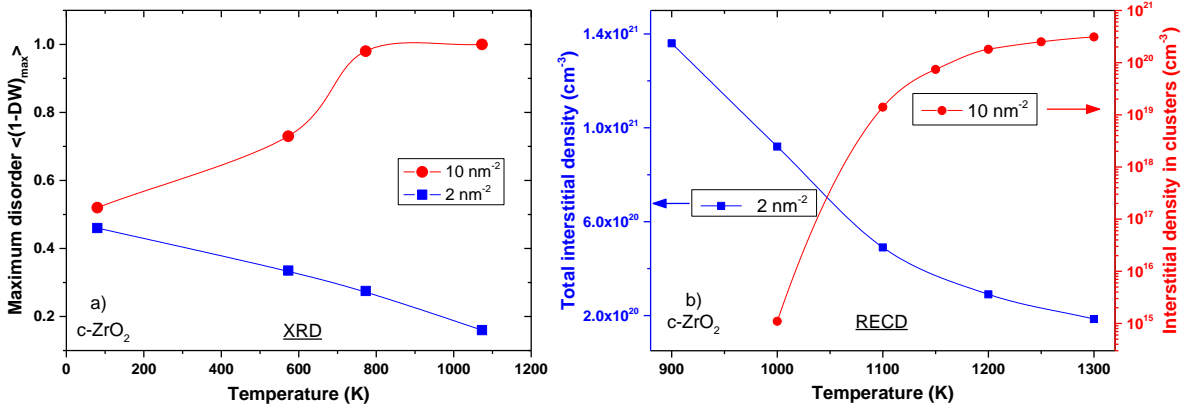

Figure 3: XRD-disorder and RECD-disorder as a function of the temperature in c-ZrO$_2$ at low and high fluences characteristic of two regimes in the damage accumulation process (see Fig. 1a).
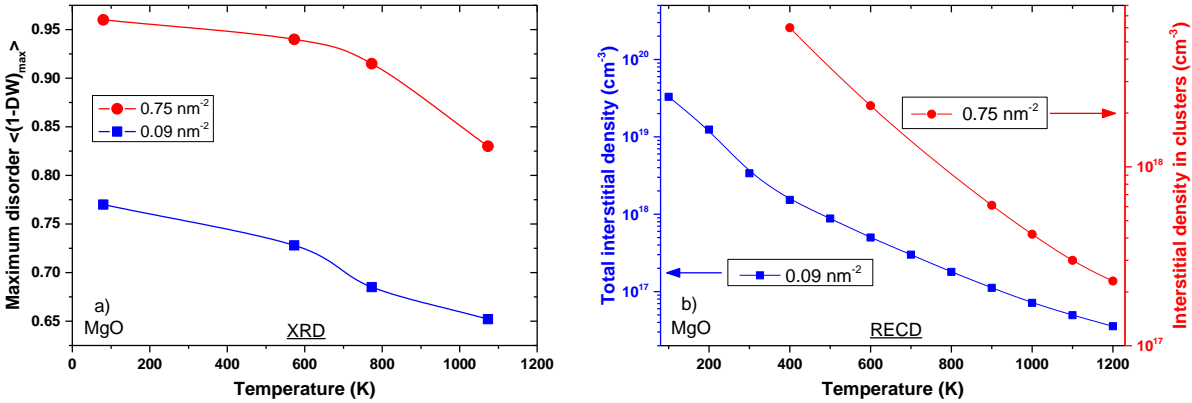

Figure 4: XRD-disorder and RECD-disorder as a function of the temperature in MgO at low and high fluences characteristic of two regimes in the damage accumulation process (see Fig. 1b).

Similarly, Fig. 4a and 4b show, for MgO, the XRD-derived and RECD-derived disorder as a function of the temperature. Experimentally, the disorder decreases with increasing temperature

irrespective of the fluence (note that the amplitude of the variations is lower than that for c-ZrO$_2$, again because of the lower intrinsic quality of the MgO single-crystals). This trend in the disorder is reproduced in the RECD simulations. In addition, the temperature range over which significant evolution in the disorder is observed match reasonably well between experiments and simulations. From these simulations, it is unambiguously demonstrated that the asymmetry in the defect mobility governs the high-temperature disorder-level, and therefore the microstructural changes, in these materials. Furthermore, this study shows that the effect of increasing the temperature during an irradiation process is definitely non-trivial and may not lead to the supposedly obvious enhancement of dynamic annealing but, depending on the defect energetics, can on the contrary accelerate microstructural changes.

In conclusion, this work reports a combined experimental (XRD) and computational (RECD) effort that aims at understanding the origin of the contrasting microstructural response of two materials, namely c-ZrO$_2$ and MgO, under irradiation over a large range of temperatures. Indeed, whereas, at a given temperature, these two oxides exhibit a very similar response to increasing ion irradiation fluence, they evolve in opposite ways with increasing temperature for a given fluence. More precisely, experiments indicate that the final defective microstructural state is reached at lower fluence in c-ZrO$_2$ as compared to MgO when the temperature is increased. In order to understand these opposite responses, we performed RECD simulations which clearly show that the defect clustering and recombination rates do depend on the defect migration energies and, critically, which mechanism dominates depends on the asymmetry in the migration of interstitials versus vacancies. Trends in the calculated levels of disorder agree well with experiment versus both fluence and irradiation temperature, indicating that the relative defect migration energy, which is the distinctive parameter in the simulations, is a key property in explaining the opposite behavior between the two oxides. Finally, this study provides an approximate yet revealing methodology for the characterization and modeling of irradiation-induced disorder.

References

[1] M. Nastasi, J. W. Mayer, J. K. Hirvonen, Ion-solid interactions: fundamentals and applications, Cambridge University Press Eds, Cambridge (1996)

[2] H. C. Huang, J. I. Dadap, G. Malladi, I. Kymissis, H. Bakhru, R. M. Jr Osgood, Helium-ion-induced radiation damage in LiNbO3 thin-film electro-optic modulators, Opt. Express 22, 19653 (2014)

[3] N. Theodoropoulou, A. F. Hebard, M. E. Overberg, C. R. Abernathy, S. J. Pearton, S. N. G. Chu, R. G. Wilson, Unconventional Carrier-Mediated Ferromagnetism above Room Temperature in Ion-Implanted (Ga, Mn)P:C, Phys. Rev. Lett. 89, 107203 (2002)

[4] A. Redondo-Cubero, K. Lorenz, S. Magalhães, E. Alves et al., Analysis of the stability of InGaN/GaN multiquantum wells against ion beam intermixing", Nanotechnology 26, 425703 (2015)

[5] T. Som, D. Kanjilal, Nanofabrication by Ion-Beam Sputtering: Fundamentals and Applications, CRC Press, Taylor and Francis Group (2012)

[6] N. Yao, Focused Ion Beam Systems, MaterialsToday **10**, 53 (2007)

[7] Y. Zhang, M. Ishimaru, T. Varga, T. Oda, C. Hardiman, H. Xue, et al., Nanoscale engineering of radiation tolerant silicon carbide, Phys Chem Chem Phys. **14**, 13429 (2012)

[8] D. V. Potapenko, Z. Li, J. W. Kysar, R. M. Osgood, Nanoscale strain engineering on the surface of a bulk TiO_2 crystal, Nanoletters **14**, 6185 (2014)

[9] R. Gupta, N. Sehdev, K. Asokan, D. Kanjilal, S. Annapoorni, Engineering strain, densification, order parameter and magnetic properties of FePt thin films by dense electronic excitations, J. Appl. Phys. **116**, 083902 (2014)

[10] H. Guo, S. Dong, Ph. D. Rack, J. D. Budai, Ch. Beekman, Z. Gai, W. Siemons, C. M. Gonzalez, R. Timilsina, A. T. Wong, A. Herklotz, P. C. Snijders, E. Dagotto, Th. Z. Ward, Strain Doping: Reversible Single-Axis Control of a Complex Oxide Lattice via Helium Implantation, Phys. Rev. Lett **114**, 256801 (2015)

[11] Y. H. Li, B. P. Uberuaga, C. Jiang, S. Choudhury, J. A. Valdez, M. K. Patel, J. Won, Y.-Q. Wang, M. Tang, D. J. Safarik, D. D. Byler, K. J. McClellan, I. O. Usov, T. Hartmann, G. Baldinozzi, K. E. Sickafus, Role of Antisite Disorder on Preamorphization Swelling in Titanate Pyrochlores, Phys. Rev. Lett **108**, 195504 (2012)

[12] G. S. Was, Z. Jiao, E. Getto, K. Sun, A. M. Monterrosaa, S. A. Maloy, O. Anderoglu, B. H. Sencer, M. Hackett, Emulation of reactor irradiation damage using ion beams, Scripta Mater. **88**, 33 (2014)

[13] N. M. Anoop Krishnan, B. Wang, Y. Yu, Y. Le Pape, G. Sant, M. Bauchy, Phys. Rev. X **7**, 031019 (2017)

[14] A. Mozumder, Y. Hatano, Charged Particle and Photon Interactions with Matter: Chemical, Physicochemical, and Biological Consequences with Applications (chapter 4), Marcel Dekker Inc Eds, New York (2004)

[15] S. J. Pearton, F. Ren, E. Patrick, M. E. Law, A. Y. Polyakov, Ionizing Radiation Damage Effects on GaN Devices, ECS Journal of Solid State Science and Technology **5**, Q35 (2016)

[16] Y. Zhang, J. Lian, C. M. Wang, W. Jiang, R. C. Ewing, and W. J. Weber, Ion-induced damage accumulation and electron-beam-enhanced recrystallization in $SrTiO_3$, Phys. Rev. B **72**, 094112 (2005)

[17] E. Wendler, Th. Bierschenk, W. Wesch, E. Friedland, J. B. Malherbe, Temperature dependence of damage formation in Ag ion irradiated 4H-SiC, NIM B **268**, 2996 (2010)

[18] J. Lian, L.M. Wang, K. Sun, R. C. Ewing, In Situ TEM of Radiation Effects in Complex Ceramics, Microsc. Res. Techn. **72**, 165 (2009)

[19] P. Kalita, S. Ghosh, G. Sattonnay, U. B. Singh, V. Grover, R. Shukla, S. Amirthapandian, R. Meena, A. K. Tyagi, D. K. Avasthi, Role of temperature in the radiation stability of yttria stabilized zirconia under swift heavy ion irradiation: A study from the perspective of nuclear reactor applications, J. Appl. Phys. **122**, 025902 (2017)

[20] L. Vincent, L. Thomé, F. Garrido, O. Kaitasov, and F. Houdelier, Microstructure of Cs-implanted zirconia: Role of temperature, J. Appl. Phys. **104**, 114904-8 (2008)

[21] D. W. Clark, S. J. Zinkle, M. K. Patel, C. M. Parish, High temperature ion irradiation effects in MAX phase ceramics, Acta Mater. **105**, 130 (2016)

[22] C. Onofri, C. Sabathier, H. Palancher, G. Carlot, S. Miro, Y. Serruys, L. Desgranges, M. Legros, Evolution of extended defects in polycrystalline UO2 under heavy ion irradiation: combined TEM, XRD and Raman study, NIM B **374**, 51 (2016)

[23] A. Debelle, J. Channagiri, L. Thomé, B. Décamps, A. Boulle, S. Moll, F. Garrido, M. Behar, J. Jagielski, Comprehensive study of the effect of the irradiation temperature on the behavior of cubic zirconia, J. Appl. Phys **115**, 183504 (2014)

[24] D. Bachiller-Perea, A. Debelle, L. Thomé, M. Behar, Damage accumulation in MgO irradiated with MeV Au ions at elevated temperatures', J. Nucl. Mater. **478**, 268 (2016)

[25] C. Degueldre, Zirconia inert matrix for plutonium utilisation and minor actinides disposition in reactors, J. Alloys and Comp. **444/445**, 36 (2007)

[26] R.R. Macdonald, M.J. Driscoll, Magnesium oxide: An improved reflector for blanket-free fast reactors, Trans. Am. Nucl. Soc. **102**, 488 (2010)

[27] E. Fabbri, D. Pergolesi, E. Traversa, Ionic conductivity in oxide heterostructures: the role of interfaces, Sci Technol Adv Mater. **11**, 054503 (2010)

[28] S. Moll, Y. Zhang, A. Debelle, L. Thomé, J.P. Crocombette, Z. Zihua, J. Jagielski, W.J. Weber, Damage processes in MgO irradiated with medium-energy heavy ions, Acta Mater. **88**, 314 (2015)

[29] Supplemental Material

[30] C.-O. Bacri, C. Bachelet, C. Baumier, J. Bourçois, L. Delbecq, D. Ledu, N. Pauwels, S. Picard, S. Renouf, C. Tanguy, Nucl. Instr. Meth. B, in press, https://doi.org/10.1016/j.nimb.2017.03.036

[31] M. Souilah, A. Boulle, A. Debelle, RaDMaX: a graphical program for the determination of strain and damage profiles in irradiated crystals, J. Appl. Cryst. **49**, 311 (2016)

[32] A. Boulle, A. Debelle, Statistical nature of atomic disorder in irradiated crystals, Phys. Rev. Lett. **116**, 245501 (2016)

[33] T. Jourdan, G. Bencteux, G. Adjanor, Efficient simulation of kinetics of radiation induced defects: A cluster dynamics approach, Journal of Nuclear Materials **444**, 298 (2014)

[34] T. Jourdan, G. Stoltz, F. Legoll, L. Monasse, An accurate scheme to solve cluster dynamics equations using a Fokker-Planck approach, Comp. Phys. Comm. **207**, 170 (2016)

[35] J.F. Ziegler, J. P. Biersack, U. Littmark, The Stopping and Range of Ions in Solids , Pergamon, New York, 1985. Available at: www.srim.org

[36] R. S. Averback, R. Benedek, K. L. Merkle, Ion-irradiation studies of the damage function of copper and silver, Phys. Rev. B 18 (1978) 4156

[37]. J.-P. Crocombette , L. Van Brutzel, D. Simeone, L. Luneville, Molecular dynamics simulations of high energy cascade in ordered alloys: Defect production and subcascade division, J. Nucl. Mater. 474, 134 (2016)

[38] M. Kilo, R. A. Jackson, G. Borchardt, Computer modelling of ion migration in zirconia, Phil. Mag. **83**, 3309 (2003)

[39] D. S. Aidhy, Y. Zhang, W. J. Weber, Radiation damage in cubic ZrO_2 and yttria-stabilized zirconia from molecular dynamics simulations, Scripta Mater. **98**, 16 (2015)

[40] B. P. Uberuaga, R. Smith, A. R. Cleave, G. Henkelman, R. W. Grimes, A. F. Voter, K. E. Sickafus, Dynamical simulations of radiation damage and defect mobility in MgO, Phys. Rev. B **71**, 104102 (2005)

[41] C. A. Gilbert, S. D. Kenny, R. Smith, E. Sanville, Ab initio study of point defects in magnesium oxide, Phys. Rev. B **76**, 184103 (2007)

[42].

[43]

[44]

[45] D. Bachiller-Perea, A. Debelle, L. Thomé, J.-P. Crocombette, Study of the initial stages of defect generation in ion-irradiated MgO at elevated temperatures using high-resolution X-ray diffraction, J. Mater. Sci. **51**, 1456 (2016)

[46] P. H. Dederichs, The theory of diffuse x ray scattering and its application to the study of point defects and their clusters, J. Phys. F: Metal Phys. **3**, 471 (1973)